

Received: / 09 May 2022 / Accepted: 22 May 2022 / Published online: 24 May 2022

*engineered parts, surface roughness,  
stress concentration,  
fatigue life*

Wit GRZESIK<sup>1\*</sup>

## **INFLUENCE OF DIFFERENT MACHINING PROCESSES ON FATIGUE LIFE PERFORMANCE OF ENGINEERED SURFACES: A SHORT REVIEW**

In this paper fundamental information on the influence of the real machined surfaces generated by different machining processes on the fatigue life of machine parts are presented. In the first part the various approaches for the assessment of the stress concentration factor and the correction of a fatigue life limit are discussed. In the second part the results of standard fatigue tests are compared with computed data and predictions using FEM based simulations. The effect of surface discontinuities (valleys) in the real surface profiles is related to engineered parts made of different materials including steels, aluminium alloys, aerospace alloys and composites.

### **1. INTRODUCTION**

The paper overviews the possible ways of the influence of surface roughness/topography produced by different machining processes on the fatigue life of machine parts which is the most important functional property by manufacturing engineering practice. Fatigue is conditioned by cyclic-plastic deformations which are controlled by two factors, i.e. plastic-strain amplitude ( $\varepsilon_a$ ) and stress amplitude ( $S_a$ ) which tend to decrease with increasing material working temperature. Some general information on the functional performance of machine parts are provided previously in Refs. [1–4]. In the group of mechanical functional properties the fatigue strength, fatigue wear (fretting) and fatigue life are distinguished [2]. In particular Ref. [1] reviews the research works on the impact of surface roughness/topography on the fatigue strength/fatigue life which are important for the design of machine parts and corresponding technological processes. In fatigue strength tests, which have a long history dating back to the second half of the nineteenth century, attention is drawn to the large number of factors affecting the durability of machine elements subjected to variable or cyclic loads, including: shape and dimensions of the element, state of its real surface, operating temperature and type of working environment [5, 6]. The fundamental assumption in this analysis is that

---

<sup>1</sup> Former affiliation: Opole University of Technology, Emeritus Professor

\* E-mail: w.grzesik@gmail.com

<https://doi.org/10.36897/jme/150322>

the surface roughness consisting of pits and troughs (equivalently summits and valleys) acts as micro-notches for cyclically loaded parts [7]. As a result, the surface condition coefficient ( $\beta_p$ ) which relates the fatigue strength of a sample with generated roughness to the fatigue strength of a smooth sample produced by a precision finishing processes, predominantly polishing is introduced [6]. Both bending and torsional loads but with a higher value of  $\beta_p$  for bending and corresponding  $R_z$  surface roughness parameter are considered. Moreover [6], the surface roughness reduction factor  $\gamma$  is defined with the same meaning as the previous coefficients. It suggests that qualitatively the fatigue life is inversely proportional to the surface roughness.

It is obviously accepted in engineering design that a surface with a  $R_z$  parameter approximately below  $2\ \mu\text{m}$  does not affect the fatigue strength of the element, while highly rough machined surfaces characterized by  $R_z = 30\div 40\ \mu\text{m}$  behave similarly as a sharp micro-notch. As a result, the real surface profile can be represented by a set of the micro-notches (valleys/grooves within the surface profile) as the inputs to the predicting of fatigue strength/life. This is because notches occurring on a rough surface increase the concentration of stresses and accelerate fatigue fracture in the areas which are mostly subjected to fatigue, predominantly in the vicinity the real machined surface [5].

The most important surface roughness parameters are selected as amplitude ( $R_a$ ,  $R_q$ ) as well as height ( $R_p$  and  $R_z$ ) and horizontal ones ( $R_{sm}$ ) [1–3, 8]. Since the distribution of the amplitude density function (ADF) is usually not Gaussian ( $R_{sk} \neq 0$ ,  $R_{ku} \neq 3$ ), it is recommended [2, 9] to consider the combined effect of the parameters  $R_{dq}$  and  $R_{ku}$  (profile slope/kurtosis). In such an approach, the stress concentration depends not only on the distribution of the profile grooves, but also on the distribution of material at the height of the surface profile (the material ratio curve).

Figure 1 illustrates the influence of the surface roughness on the localization of the Wöhler curve (so-called stress-cycle (S-N) function) within the  $\sigma_a-N_f$  envelope.

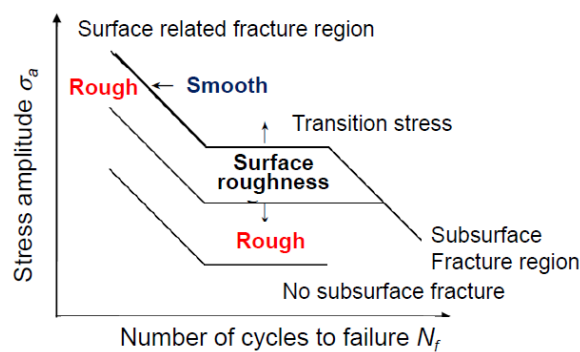


Fig. 1. Schematic illustration of the effects of surface roughness on S-N characteristics of high-strength steels [8]

On the other hand, Fig. 2 presents the relationship  $N_f = f(R_a)$  which expresses the effect of the  $R_a$  roughness parameter on LCF (low cycle fatigue), i.e. number of cycles leading to fatigue fracture. In this case, the experimental data fits the power function in the form of  $N_f = 2559 \times R_a^{-0.1166}$ . It is important to note that the optimal surface roughness of the parts subjected to variable loads is within the range  $R_a = 0.2\text{--}0.6\ \mu\text{m}$ .

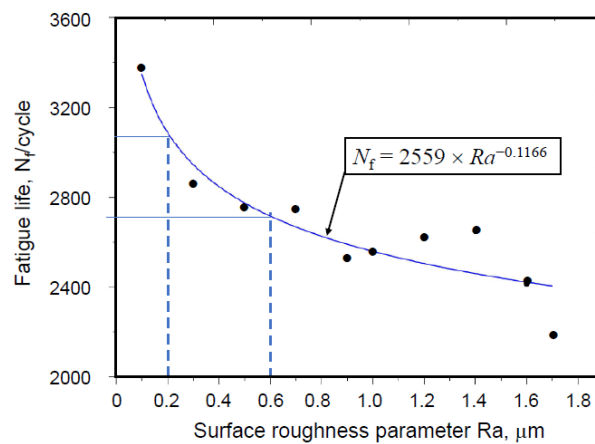


Fig. 2. Impact of surface roughness on fatigue life of an alloy steel ( $Y = 420$  MPa) [3, 10]

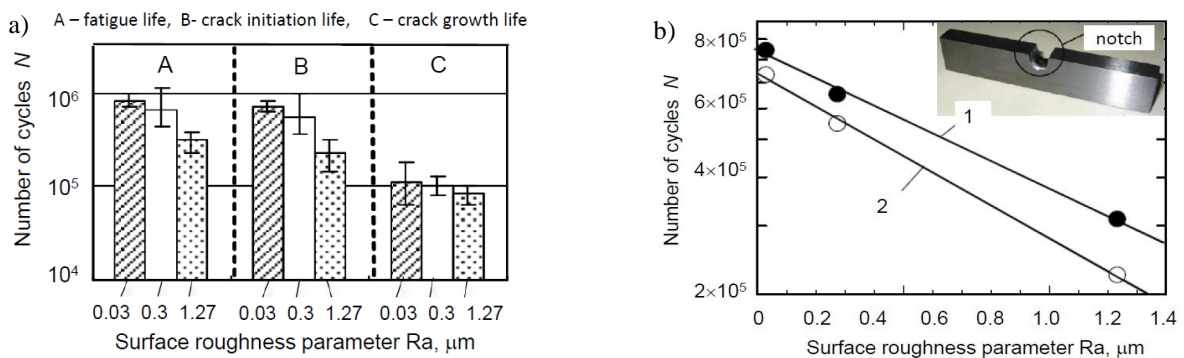


Fig. 3. Influence of average roughness  $Ra$  on number of cycles for bending fatigue tests under the bending stress  $\sigma_b = 800$  MPa (30 Hz) (a) and comparison of the fatigue life and crack initiation life vs. surface roughness (b): 1 – fatigue life, 2 – crack initiation life [3, 11]

As shown in Fig. 3a, for rough surfaces, it should be distinguished between the classic fatigue life ( $N_f$  – symbol A), the crack initiation life (B) and the crack growth life (C). However, the crack initiation life predominantly determines the fatigue life since the crack initiation life shares over 90% of the fatigue life (Fig. 3a). In this study, notches were prepared on sample surfaces with roughness values of  $Ra = 0.03$  and  $0.30$  and  $1.27$   $\mu\text{m}$  respectively. The signal of crack initiation was detected by measuring the resistance of a thin silver (Ag) film deposited on the sample by ion-sputtering. The straight lines in the graph shown in Fig. 3b were obtained based on bending tests ( $\sigma_b = 800$  MPa, maximum load  $F_{\text{max}} = 6500$  N) of notched samples made of non-alloyed steel S55C JIS with a hardness of 180–230 HB [11]. Their inclinations indicates that rougher surfaces has significantly shorten the fatigue life and should be considered in the practical approach to the prediction of fatigue life.

## 2. ANALYTICAL AND NUMERICAL METHODS FOR ASSESSING THE IMPACT OF SURFACE NOTCHES ON FATIGUE LIFE

In practical design rules the influence of macroscopic geometric surface features on the fatigue strength of machine parts is usually expressed by means of the fatigue stress

concentration coefficient ( $K_t$ ) [12], given originally by Pedersen. It was related to a single notch characterized by the notch height  $t$  and the notch root radius  $\rho$  (Fig. 4) as variable factors. In order to cover a number of the surface pits the real machined surface cover multiple notches as shown in Fig. 4 (lower figure). As a result, the fatigue stress concentration coefficient ( $K_t$ ) should be expressed in terms of a representative 2D or 3D standardized surface roughness parameter.

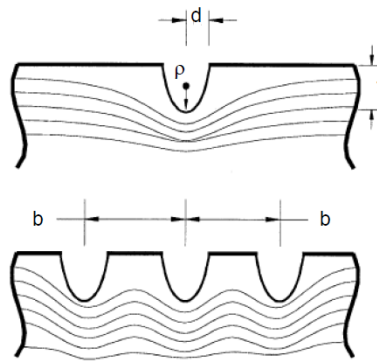


Fig. 4. Schematic illustration of the stress concentration for single (upper) and multiple notches (lower) [12]

The first approach was the semi-empirical formula (1) [12] by Neuber in which the average notch height on a rough surface  $t$  is replaced by the maximum height of the surface profile  $Rz$  measured for the real surface profile, as

$$K_t = 1 + n \sqrt{\lambda \frac{Rz}{\rho}} \quad (1)$$

where:  $n$  – stress state coefficient (in Ref. [10] it was assumed to be equal to 2),  $Rz$  – maximum height of the surface roughness profile on the elementary length,  $\lambda$  – ratio of the spacing to the height of asperities/micro-irregularities in the analysed surface profile ( $\lambda = b/t$  in Fig. 4),  $\rho$  – average radius of the profile valley.

Usually, the coefficient  $\lambda = 1$ , which is explained by the difficulties of unambiguous interpretation, while the coefficient  $n$  is taken as 1 for shear and 2 for uniform tension loads.

An alternative expression (2a) for the effective stress concentration to formula (1) was proposed by Arola [12, 13]. In particular, it was selected as an important heredity index describing functional properties of the machined surfaces [7].

$$K_{t,2} = 1 + n \frac{Ra \cdot Rt}{\rho_v \cdot Rz} \quad (2a)$$

where:  $Ra$  – the average roughness of the surface,  $Rt$  – maximum roughness height on the measuring length,  $Rz$  – maximum roughness height on the elementary section,  $\rho_v$  – effective radius from the dominant profile valleys.

In order to increase the accuracy of the prediction, it is recommended [14] to replace 2D roughness parameters ( $Ra$ ,  $Rz$  and  $Rt$ ) by analogous 3D parameters ( $Sa$ ,  $Sz$  and  $St$ ). As a result, the stress concentration coefficient can be determined as follows:

$$K_{t,3} = 1 + n \frac{Sa \cdot St}{\rho_v \cdot Sz} \quad \text{or} \quad K_{t,3} = 1 + n \frac{Sa(Sp_{\max} + Sv_{\max})}{\rho_v \cdot Sz} \quad (2b)$$

where:  $Sp_{\max}$  – height of the highest surface peak,  $Sv_{\max}$  – depth of the lowest surface valley.

For the experimentally determined stress concentration factor  $K_t$  the equivalent fatigue stress concentration factor  $K_f$  is determined [12] using the following formulas:

- in general form

$$K_f = \frac{\sigma_{D(\text{smooth})}}{\sigma_{D(\text{rough})}} \quad (3a)$$

- in a form related to an equivalent surface notch

$$K_f = 1 + q(K_t - 1) \quad (3b)$$

here:  $\sigma_{D(\text{smooth})}$  – allowable stress for a smooth sample (with no notch),  $\sigma_{D(\text{rough})}$  – allowable stress for a rough sample (with notch),  $q$  – notch sensitivity factor.

In turn, the coefficient  $q$  is defined depending on the effective radius of the surface valley ( $\bar{\rho}$ ) instead of the radius of a single notch  $\rho$ , i.e.

$$q = \frac{1}{1 + \gamma/\bar{\rho}} \quad (4)$$

where:  $\gamma$  – material constant depending on the ultimate tensile strength (UTS) determined for steels from the following expression

$$\gamma = 0.025 \left( \frac{2070 \text{ MPa}}{UTS} \right)^{1.8} [\text{mm}], \quad UTS \geq 550 \text{ MPa}. \quad (5)$$

Value of the stress concentration coefficient can be determined analytically assuming circular or elliptic micro-notches repeating on the surface or using the finite element method (FEM) in relation to the filtered surface profile – as shown in Fig. 5.

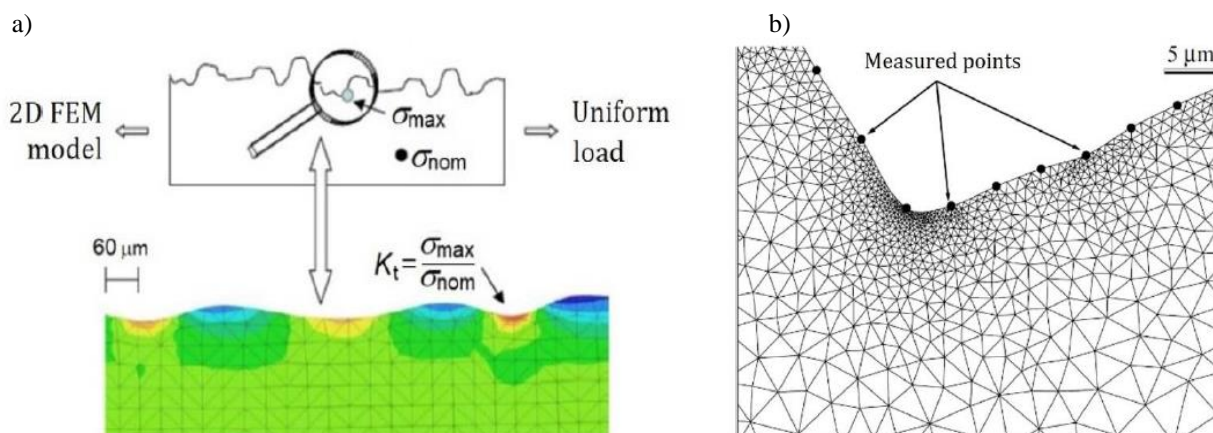


Fig. 5. Principle of numerical calculations of the stress concentration coefficient (a) [13] and a FEM mesh within a notch (b) [14]

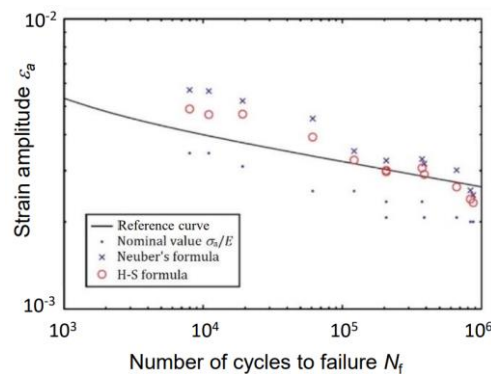


Fig. 6. Comparison of the determined fatigue life predicted empirically and analytically [3, 14]

A fragment of the valley of the roughness profile obtained from 3D measurements of the surface with the applied finite element mesh is shown in Fig. 5b. The smallest mesh size was about  $0.1 \mu\text{m}$ . The groove profile was obtained by interpolation with a Bézier curve, and the mesh elements were shaped as triangular axisymmetric elements. The points on the groove outline represent the results of the WLI (white light interferometer) measurements carried out on the interferometer. For all grooves on which crack initiation was observed, the strain amplitude  $\varepsilon_a$  was determined with the correction given by Neuber according to the formula (1) and Hoffmann-Seeger (H-S) according to the formula:

$$K_f = \frac{K_t}{1 + \sqrt{c\chi}} \quad (6)$$

where:  $c$  – material constant,  $\chi$  – stress gradient.

The simulation results, presented in Fig. 6, indicate that roughness can even reduce the fatigue life by up to 10 times [14]. The strain amplitudes were calculated by means of formulas (1) and (6) using the median value of  $c$ . It is confirmed that the Neuber formula (1) better predicts high-cycle fatigue (HCF).

### 3. PREDICTION OF THE IMPACT OF SURFACE MICRO-NOTCHES ON FATIGUE LIFE

Methodology for determining the effect of surface roughness on fatigue strength/life, based on the empirical method of assessing the impact of micro-notches, was verified for AISI 4130 CR alloy steel [10, 12],  $(\alpha+\beta)$  titanium alloy Ti-6Al-4V [15], aluminum alloy 7010 – T7451 [16], A357 aluminum alloy produced by the additive method (SLM) [17], nickel-based super alloy alloy 720Li [18] and laminate reinforced with graphite fibers [13].

Figure 7 shows a flat sample made of Ti-6Al-4V titanium alloy (detail within Fig. 7) after end milling operation ( $v_c = 20\text{--}110 \text{ m/min}$ ,  $f_z = 0.02\text{--}0.05 \text{ mm/tooth}$ ,  $a_e = 0.5\text{--}2.0 \text{ mm}$ ) and a representative roughness profile recorded on the neck surface with a defined valley (micro-notch) radius. The side surface (SS) of the fatigue specimen was processed by end-milling, grinding and polishing and the investigated neck surface (NS) was machined by peripheral milling.

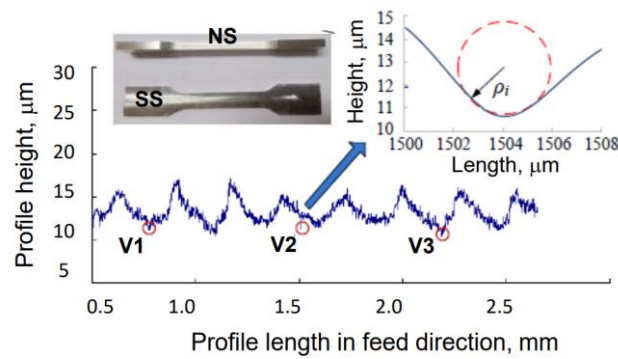


Fig. 7. View of the specimen for fatigue testing and determining representative valley radii within recorded profile [15]

Corresponding fatigue tests were carried out for the stress ratio ( $R = \sigma_{\min}/\sigma_{\max}$ )  $R = 0.1$  and the maximum stress value  $\sigma_{\max} = 1000$  MPa, which is slightly higher than the yield strength ( $Y=894\text{--}903$  MPa) of the titanium alloy. The measured values of the radius of valleys of micro-irregularities for various milling conditions ( $\rho = 1.50\text{--}7.10$   $\mu\text{m}$  in Fig. 7) were used to calculate the coefficients  $K_{t,2}$  and  $K_{t,3}$  (i.e. for profile and surface topography respectively) according to formulas (2a) and (2b). As a result, three mathematical models determining the influence of  $K_t$  factor and milling parameters on fatigue life  $N_f$  were determined as

$$N_{f,2} = 6695.7 \cdot K_{t,2}^{-0.531} \quad (7a)$$

$$N_{f,3} = 11071.7 \cdot K_{t,3}^{-1.056} \quad (7b)$$

$$N_f = 624.02 \cdot v_c^{-0.0469} f_z^{-0.681} \cdot a_e^{0.0152}. \quad (7c)$$

It was found that the number of cycles to material failure did not exceed 103 [15].

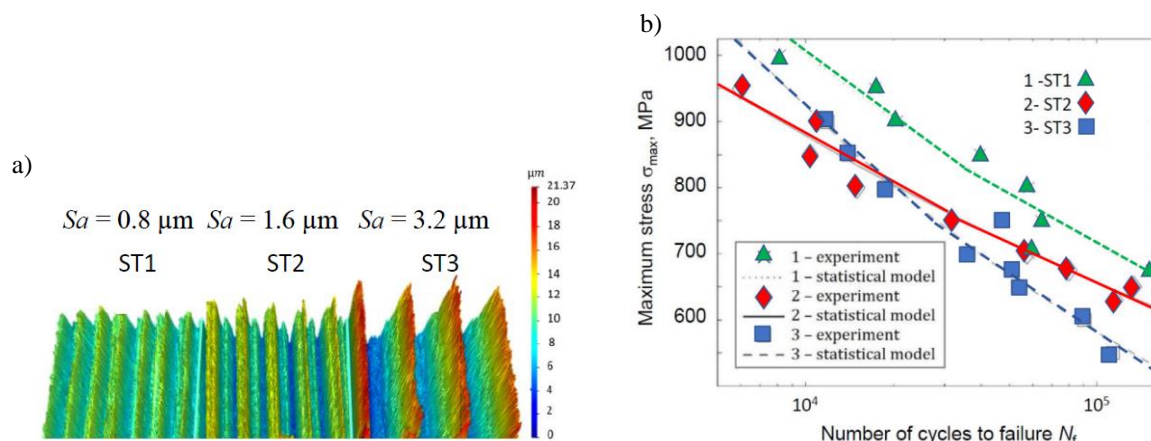


Fig. 8. A series of surface topographies of the turned samples with different surface topographies ST1, ST2 and ST3 (values of  $Sa$  surface roughness parameter for fatigue tests) (a) and corresponding S-N chart for low-cycle fatigue (b) [3, 16]

Figure 8a presents zoomed series of surface topographies of the turned surface generated on the nickel-based alloy 720Li workpieces, which is used on the elements of aircraft turbine rotors operating under high fatigue loads below  $10^5$  cycles [15]. The tests were carried out for

samples with different surface roughness of  $Sa = 0.8 \mu\text{m}$ ,  $1.6 \mu\text{m}$  and  $3.2 \mu\text{m}$ , subjected to trapezoidal (LCF) and sinusoidal (HCF) loads. Samples were cut from the discs in the radial direction by means of WEDM.

S-N charts obtained for low cycle life (Fig. 8b) show slight differences due to deterioration resulting from surface roughness for large maximum stress values, rather due to the dispersion of results. They are larger when the number of cycles increases to  $10^5$  (fatigue life is about 10% lower for a sample with a higher surface roughness). A noticeable border between the different effects of surface roughness (runs 2 and 3 in Fig. 9b) occurs for a stress of about 750 MPa. In turn, for high cycle life – over  $10^6$  cycles – the effect of surface roughness clearly disappears.

Based on fractional fracture studies, it was found that multiple fatigue cracks appear within the valleys of micro-irregularities, and therefore the assessed effect of surface roughness is topological ( $K_t > 1.0$ ) [16]. It is suggested to involve other spatial parameters, such as  $S_v$ , and hybrid parameters –  $Sdq$ ,  $Ssc$  and  $Sdr$ . Their definitions are given in Ref. [19].

Figure 9a shows a fragment of the surface profile obtained for a sample made of AISI 4130 CR alloyed steel ( $R_m = 752 \text{ MPa}$ ,  $R_e = 655 \text{ MPa}$ ) after abrasive water jet machining (symbol C in Fig. 9a corresponds to the valley when the surface roughness  $Ra = 6 \mu\text{m}$ ) was investigated. The mean measured values of the valley radius of the pit were  $10.8 \mu\text{m}$ ,  $9.2 \mu\text{m}$  and  $9.0 \mu\text{m}$ , respectively.

The resulting S-N graph is shown in Fig. 9b. It should be noted that the border between LCF and HCF occurs approximately for the stress amplitude  $\sigma_a = 315 \text{ MPa}$  ( $N_f = 10^4$  cycles). It was found that sample C with the surface with the highest roughness ( $Ra = 6 \mu\text{m}$ ) showed the highest strength in the low cycle range – for  $N \leq 10^4$  cycles. In turn, reducing the roughness to  $Ra = 2 \mu\text{m}$  results in greater life in the high cycle range (over  $10^6$  cycles). It is worth noting that the change in surface roughness does not significantly affect the value of the notch sensitivity factor ( $q = 0.057\text{--}0.067$ ). Based on fractographic studies, it has been shown that in the low-cycle range, fatigue cracking is caused by geometric discontinuities within the profile valley, and in the high-cycle range, ductile fracture dominates (profile geometric discontinuities are of secondary nature here).

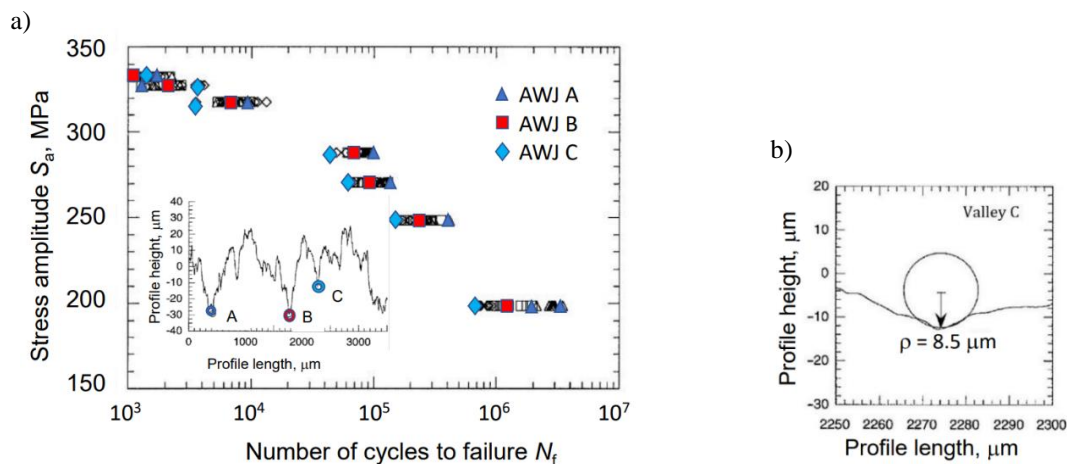


Fig. 9. The S-N graph for LCF and HCF fatigue testing (a) and determining representative valley radii within recorded profile (b) [15]

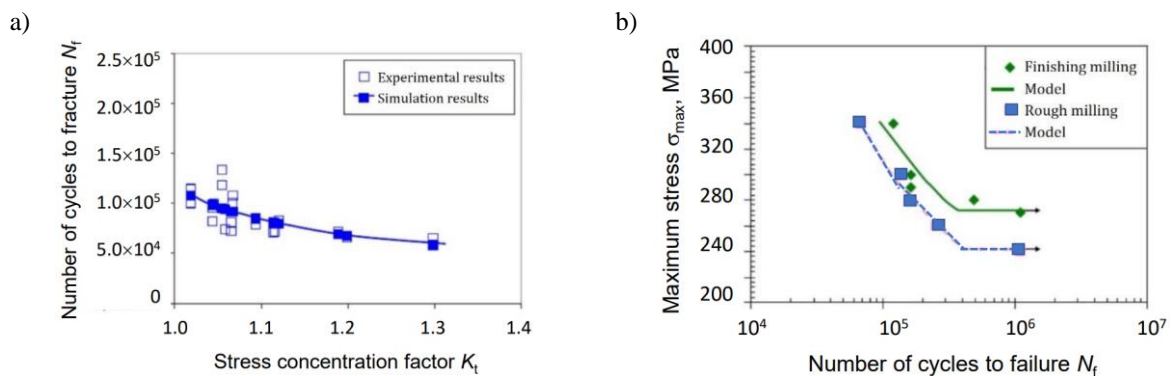


Fig. 10. Dependence of fatigue life on the factor  $K_t$  (a) and comparison of FEM simulation results with experimental data obtained for milling operations (b) [3, 18]

In the case of identical processing of the Gr/Bmi (graphite/bismaleimide resin) laminate reinforced with IM-7 carbon fibers, significantly greater radii of valleys of irregularities were obtained (e.g.  $\rho = 18 \mu\text{m}$  for roughness parameter  $Ra = 2 \mu\text{m}$  and  $\rho = 65 \mu\text{m}$  for roughness parameter  $Ra = 10 \mu\text{m}$ ), which means that the corresponding values of the  $K_f$  coefficient for double-sided bending are equal to 0.75 and 0.90 [13]. Hence, the increase in the surface roughness reduces the laminate rigidity under variable load conditions.

Figure 10a shows the result of the simulation of fatigue life as a function of the coefficient  $K_t$  for the maximum von Mises stress of 320 MPa. To validate the simulation results, fatigue tests were carried out for a load factor of  $R = 0.1$  and a frequency of 10 Hz [18]. Figure 10b shows a clear boundary between the areas belonging to LCF and HCF, corresponding to the number of cycles of about  $3 \times 10^5$ . The corresponding S-N curves show that the effect of surface roughness is more visible for  $N_f > 3 \times 10^5$  cycles. Figure 10b compares the results of FEM simulation (according to the methodology presented in fig. 6) with experimental data for samples made of aluminum alloy 7010-T7451 (Al-Cu-Mg) after finishing end-milling and roughing ball-end milling. The surface roughness  $Ra$  varied in the range from  $0.25 \mu\text{m}$  to  $11 \mu\text{m}$ , which results in the corresponding values of the stress concentration coefficient determined from the formula (2a) equal to  $K_t = 1.022$  and  $K_t = 1.154$  (Fig. 10a).

Figure 11 shows a comparison of fatigue strength of samples from aluminum alloy A357 fabricated by the selective laser melting (SLM) in the initial state ( $Ra \approx 7 \mu\text{m}$ ,  $Rz \approx 60 \mu\text{m}$ ) and after additional machining ( $Ra \approx 0.2 \mu\text{m}$ ) and samples fabricated by pressure castings. Figure 11 depicts that precision machining causes that the fatigue life increases, especially in the case of lower stress values, which can be explained by the fact that in the sintered materials fatigue crack propagation occurs at higher stresses. A fatigue life comparable to that of as-cast samples is determined. However, it is important to emphasize that both surface and subsurface defects as well as high residual stresses induced by the cutting process cause the large variation of experimental results. An important finding from the fatigue strength tests of the Ti-6Al-4V titanium alloy fabricated by the STM method and then finished by turning and milling, and polishing, was the lack of correlation with the roughness parameter  $Sa$  [20]. In turn, the fatigue strength was sensitive to changes in skewness  $Ssk$  because surfaces with  $Ssk > 0$  work better under cyclical loads. However, the fatigue strength for AM made samples is about two times lower than for cast samples.

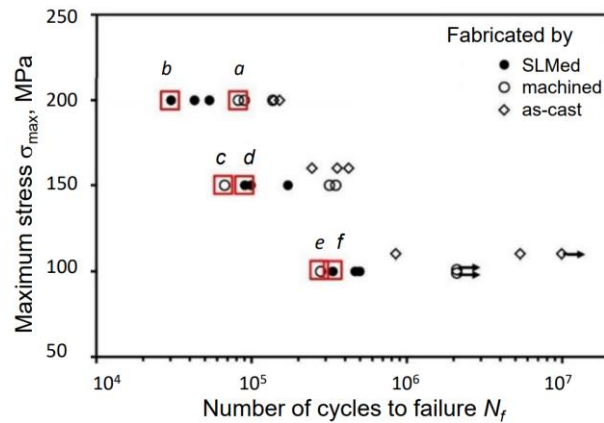


Fig. 11. Impact of manufacturing processes on the fatigue strength of A357 aluminium alloy produced by the SLM method [17]. Symbols *a-f* denote various types of crack propagation mechanisms

#### 4. GENERAL TRENDS IN THE INFLUENCE OF PROCESS CONDITIONS ON THE MICRO-CRACKS DEVELOPMENT

Surface integrity is closely related with the functional performance of machined parts. Moreover, it is well known in the mechanical engineering practice that surface roughness is an important factor influencing the growth and nucleation of fatigue cracks. Therefore, reducing the strength/fatigue life in terms of the surface roughness reduction factor  $\gamma$  is an approximate solution, because the surface roughness may differ for the same machining conditions, and the measurement of the surface roughness itself may be affected by a large error. An important question arises whether the same value of  $\gamma$  factor is ensured for the notched surface, because the roughness effect is superimposed to the notch effect. In practical terms, the sensitivity of fatigue strength to the surface roughness (in general surface topography) increases when machining the high-strength material, as for instance for hardened steels and precipitation hardened aluminum alloys [7, 8]. For this reason, it is recommended to consider the influence of the structural notch (lower index: *notch*) by the interaction of surface micro-notches (lower index: *sr*), i.e. use the correction coefficient as follows:

$$K_t = (K_t)_{\text{notch}} \times (K_t)_{\text{sr}} \quad (8)$$

Special surface strengthening processes such as severe plastic deformation, phase transformation and alloying are not included in the study, although they are often used in practice [21]. Information on strengthening machine parts by surface strain-hardening using hybrid processes with controlled mechanisms such as ball burnishing process and its influence on the fatigue strength is presented in Ref. [22].

In order to improve fatigue performance a number of mechanical surface treatments such as shot or laser shock peening, deep rolling and burnishing are employed. Figure 12 presents some important alterations in the machined surface and the subsurface layer (SL), taking into account smoothing of the machined surface, material strain-hardening and the presence of compressive residual stress, i.e. main factors determining the nucleation and propagation of fatigue cracks.

SL modifications		FC nucleation		FC propagation
Compressive residual stresses		Minor or no effect		Retards
SL strain-hardening	→	Retards	→	Accelerates
Surface roughness		Accelerates		No effect

Fig. 12. Effects of surface layer (SL) properties on the formation of fatigue cracks (FC) [8]

It should be noted, however, that their impact is definitely different. For instance, the strain-hardening retards the nucleation but accelerates the propagation of fatigue cracks. For instance, ball burnishing of hardened 41Cr4 alloy steel reduces the fatigue stress concentration factor from about  $K_t = 1.8$  for initially turned surface to about 1.3 after single-pass burnishing operation [7].

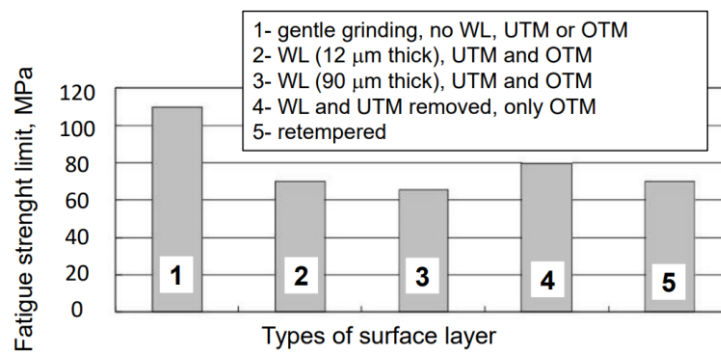


Fig. 13. The influence of the SL alterations on fatigue strength [8]. Symbols: UTM – untampered martensite, OTM – overtempered martensite, WL – white layer

In practice, the fatigue strength is associated with basic surface integrity factors, such as high temperature and high temperature gradients, metallurgical alterations including untampered martensite (UTM) and overtempered martensite (OTM), plastic deformation and chemical changes. The abusive machining operations can produce UTM and OTM with a corresponding strain-hardening and subsurface material softening. As shown in Fig. 13, these metallurgical alterations generated during machining processes have a detrimental effect on fatigue durability of the machined parts.

## 5. MAIN CONCLUSIONS

In general, it is possible to assess the fatigue life of the machined parts with defined characteristics of surface integrity. The fundamental assumption in this analysis is that the surface roughness consisting of pits and troughs (equivalently summits and valleys) acts as micro-notches for cyclically loaded parts. Also strain-hardening effect, residual stresses and metallurgical alterations such as phase transformation influence the fatigue life/fatigue strength.

The influence of surface roughness should be related not only to the fatigue life but also to crack initiation life. As a result, the fatigue stress concentration coefficient ( $K_t$ ) and the equivalent fatigue stress concentration factor ( $K_f$ ) should be expressed in terms of a representative 2D or 3D standardized surface roughness parameter.

Fatigue life can be predicted by means FEM methods based on the recorded surface profile and corresponding surface roughness parameters  $R_a$  and  $R_z$  (equivalent 3D SR parameters) and representative valley radii  $\rho_v$  within recorded profile.

It should be taken into account that corresponding alterations in the machined surface and the subsurface layer (SL) result in smoothing of the machined surface, material strain-hardening and the presence of compressive residual stress, i.e. main factors determining the nucleation and propagation of fatigue cracks. It should be noted, however, that their impact is definitely different.

#### REFERENCES

- [1] GRZESIK W., 2016, *Prediction of the Functional Performance of Machined Components Based on Surface Topography: State of the Art*, Journal of Materials Engineering and Performance, 25/10, 4460–4468.
- [2] GRZESIK W., 2016, *Influence of Surface Textures Produced by Finishing Operations on their Functional Properties*, Journal of Machine Engineering, 16/1, 15–23.
- [3] GRZESIK W., 2019, *Influence of Surface Roughness on Fatigue Life of Machine Elements – Developments in Experimental Investigations and Simulation*, Mechanik, 5–6, <https://doi.org/10.17814/mechanik.2019.5–6.39>.
- [4] HASHIMOTO F., CHAUDHARI R.G., MELKOTE S.N., 2016, *Characteristics and Performance of Surfaces Created by Various Finishing Methods*, Procedia CIRP, 45, 1–6.
- [5] KOCANDA S., KOCANDA A., 1989, *Low-Cycle Fatigue Strength of Metals*, PWN, Warsaw, (in Polish).
- [6] SCHIJVE J., 2009, *Fatigue of Structures and Materials*, Milton Keynes, Springer.
- [7] GRZESIK W., ZAK K., CHUDY R., PRAZMOWSKI M., MALECKA J., 2019, *Optimization of Subtractive-Transformative Hybrid Processes Supported by the Technological Heredity Concept*, CIRP Annals – Manufacturing Technology 68, 101–104.
- [8] GAO S., ZHANG Q., 2013, *Influence of Machined Surface Integrity on Fatigue Performance*, Applied Mechanics and Materials, 373–375, 1999–2003.
- [9] NOVOCIC D., DEWES R.C., ASPINWALL D.K., VOICE W., BOWEN P., 2004, *The Effect of Machined Topography and Integrity on Fatigue Life*, International Journal of Machine Tools and Manufacture, 44/2–3, 125–134.
- [10] XIAO W.L., CHEN H.B., YIN Y., 2013, *Effects of Surface Roughness on the Fatigue Life of Alloy Steel*, Applied Mechanics and Materials, 373–375, 417–420.
- [11] DENG G., NAGAMOTO K., NAKANO Y., NAKANISHI T., 2009, *Evaluation of the Effect of Surface Roughness on Crack Initiation Life*, Proceedings of 12th International Conference on Fracture (ICF12), Ottawa, Canada, 2, 1505–1512.
- [12] AROLA D., WILLIAMS C.L., 2002, *Estimating the Fatigue Stress Concentration Factor of Machined Surfaces*, International Journal of Fatigue, 24, 923–930.
- [13] AROLA D., WILLIAMS C.L., 2002, *Surface Texture, Fatigue, and Reduction in Stiffness of Fiber Reinforced Plastics*, Transactions of the ASME, Journal of Engineering Materials and Technology, 124, 160–166.
- [14] AS S.K., SKALLERUD B., TVEITEN B.W., HOLME B., 2005, *Fatigue life Prediction of Machined Components Using Finite Element Analysis of Surface Topography*, International Journal of Fatigue, 27, 1590–1596.
- [15] YANG D., LIU Z., XIAO X., XIE F., 2018, *The Effects of Machining-Induced Surface Topography on Fatigue Performance of Titanium Alloy Ti-6Al-4V*, Procedia CIRP, 71 27–30.
- [16] SURARATCHAI M., LIMIDO J., MABRU C., CHIERAGATTI R., 2008, *Modelling the Influence of Machined Surface Roughness on the Fatigue Life of Aluminium Alloy*, International Journal of Fatigue, 30, 2119–2126.
- [17] RAO J.H., ZHANG K., ROMETSCH P., HUANG A., WU X., 2018, *The Influence of Surface Roughness on the Fatigue Performance of Selective Laser Melted Aluminium Alloy A357*, Proceedings of the 16th International Aluminium Alloys Conference (ICAA16), Canada.
- [18] ARDI D.T., LI Y.G., CHAN K.H., BLUNT L., BACHE M.R. 2014, *The Effects of Machined Topography on Fatigue Life of a Nickel Based Superalloy*, Procedia CIRP, 13, 19–24.
- [19] LEACH R. (ed.), 2013, *Characterization of Areal Surface Texture*, Springer, Heilderberg.

- [20] DUMAS M., CABANETTES F., KAMINSKI R., VALIORGUE F., PICOT E., LEFEBVRE F., GROSJEAN C., RECH J., 2018, *Influence of the Finish Cutting Operations on the Fatigue Performance of Ti-6Al-4V Parts Produced by Selective Laser Melting*, *Procedia CIRP*, 71, 429–434.
- [21] BURAKOWSKI T., 2013, *Areology. Theoretical Fundamentals*, Scientific Publ. of ITE, Radom, (in Polish).
- [22] GRZESIK W., RUSZAJ A., 2021, *Hybrid Manufacturing Processes*, PWN, Warsaw, (in Polish).